

# The Effects of Crystallinity on Charge Transport and the Structure of Sequentially Processed F<sub>4</sub>TCNQ-Doped Conjugated Polymer Films

D. Tyler Scholes, Patrick Y. Yee, Jeffrey R. Lindemuth, Hyecheon Kang, Jonathan Onorato, Raja Ghosh, Christine K. Luscombe, Frank C. Spano, Sarah H. Tolbert,\* and Benjamin J. Schwartz\*

The properties of molecularly doped films of conjugated polymers are explored as the crystallinity of the polymer is systematically varied. Solution sequential processing (SqP) was used to introduce 2,3,5,6-tetrafluoro-7,7,8,8-tetracyanoquinodimethane (F<sub>4</sub>TCNQ) into poly(3-hexylthiophene-2,5-diyl) (P3HT) while preserving the pristine polymer's degree of crystallinity. X-ray data suggest that F<sub>4</sub>TCNQ anions reside primarily in the amorphous regions of the film as well as in the P3HT lamellae between the side chains, but do not  $\pi$ -stack within the polymer crystallites. Optical spectroscopy shows that the polaron absorption redshifts with increasing polymer crystallinity and increases in cross section. Theoretical modeling suggests that the polaron spectrum is inhomogeneously broadened by the presence of the anions, which reside on average 6–8 Å from the polymer backbone. Electrical measurements show that the conductivity of P3HT films doped by F<sub>4</sub>TCNQ via SqP can be improved by increasing the polymer crystallinity. AC magnetic field Hall measurements show that the increased conductivity results from improved mobility of the carriers with increasing crystallinity, reaching over 0.1 cm<sup>2</sup> V<sup>-1</sup> s<sup>-1</sup> in the most crystalline P3HT samples. Temperature-dependent conductivity measurements show that polaron mobility in SqP-doped P3HT is still dominated by hopping transport, but that more crystalline samples are on the edge of a transition to diffusive transport at room temperature.

drop-casting, and blade-coating can be used to create reproducible active layers for organic electronic devices.<sup>[1–7]</sup> As with traditional inorganic semiconductors, the electronic properties of semiconducting polymers can be effectively tuned through doping,<sup>[8–13]</sup> by either removing (p-type doping) or adding (n-type doping) an electron to the polymer backbone. One of the most common ways to dope a semiconducting polymer is via the use of a molecular dopant, such as a small molecule, that can reduce or (much more commonly) oxidize the polymer backbone.<sup>[8,14–19]</sup> Indeed, the addition of small amounts of molecular dopants can improve the performance of polymer-based bulk heterojunction solar cells as the doped carriers fill intrinsic traps,<sup>[20–24]</sup> and more extensive molecular doping can vastly improve conductivity and carrier mobility for transistor<sup>[13,25]</sup> or thermoelectric<sup>[26,27]</sup> applications. Common p-type molecular dopants for semiconducting polymers include iodine (I<sub>2</sub>),<sup>[28–30]</sup> iron chloride (FeCl<sub>3</sub>),<sup>[17,31]</sup> and 2,3,5,6-tetrafluoro-7,7,8,8-tetracyanoquinodimethane (F<sub>4</sub>TCNQ).<sup>[11,32,33]</sup>

Because of the large advantages offered by molecular doping, there has been a great deal of work done to characterize the structural, optical, and electronic properties of doped semiconducting polymers as a function of the degree of molecular

## 1. Introduction

One of the greatest advantages of organic electronics based on semiconducting polymers is the ease of device manufacturing through solution processing: techniques such as spin-coating,

D. T. Scholes, P. Y. Yee, H. Kang, Prof. S. H. Tolbert, Prof. B. J. Schwartz  
Department of Chemistry and Biochemistry  
University of California  
Los Angeles, Los Angeles, CA 90095-1569, USA  
E-mail: tolbert@chem.ucla.edu; schwartz@chem.ucla.edu

Dr. J. R. Lindemuth  
Lake Shore Cryotronics  
Westerville, OH 43082, USA

J. Onorato, Prof. C. K. Luscombe  
Materials Science and Engineering Department  
University of Washington  
Seattle, WA 98195-2120, USA

R. Ghosh, Prof. F. C. Spano  
Department of Chemistry  
Temple University  
Philadelphia, PA 19122, USA

Prof. S. H. Tolbert  
Department of Materials Science and Engineering  
University of California  
Los Angeles, Los Angeles, CA 90095, USA

Prof. S. H. Tolbert, Prof. B. J. Schwartz  
California NanoSystems Institute  
University of California  
Los Angeles, Los Angeles, CA 90095, USA

 The ORCID identification number(s) for the author(s) of this article can be found under <https://doi.org/10.1002/adfm.201702654>.

DOI: 10.1002/adfm.201702654

doping.<sup>[8,11,17,29,34–44]</sup> There has been much less work, however, aimed at studying how systematically varying the structure or degree of crystallinity of a conjugated polymer affects the properties of the chemically doped material.<sup>[40,45–48]</sup> One reason for this is that in many cases, molecular doping is performed in solution. The dopant and polymer are co-dissolved in what is typically a good solvent for the polymer, but as the dopant oxidizes the polymer, it becomes electrically charged and thus much less soluble in the nonpolar solvents typically used for semiconducting polymers. Thus, the structures of doped polymer films cast from such solutions are determined primarily by aggregation of the doped polymer and the choice of solvent, and the film quality is generally quite poor.<sup>[43,46,47,49–51]</sup> Postdoping processing methods to improve crystallinity, such as thermal annealing, also can be problematic, as exposure to increased temperatures can de-dope conjugated polymer films.<sup>[31,47,52,53]</sup>

To avoid issues with poor film quality at high doping levels, there has been a recent thrust in the literature to utilize methods where the dopant is applied to a precast film of the undoped semiconducting polymer. Techniques include relying on exposing a conjugated polymer film to a dopant in the vapor phase,<sup>[12,17,27,36]</sup> employing solid-state diffusion to infiltrate a molecular dopant into a conjugated polymer film,<sup>[54]</sup> soaking a conjugated polymer film in a dopant solution for extended time,<sup>[17,29,55]</sup> or using solution sequential processing (SqP), where a solution of the dopant is spin-cast directly onto an undoped conjugated polymer film.<sup>[47]</sup> Our group has performed a great deal of work characterizing the SqP method, which we originally developed for inserting fullerenes into precast conjugated polymer films to produce bulk heterojunction (BHJ) solar cells.<sup>[56–59]</sup> The SqP technique, however, is applicable to infiltration of any small molecule into a polymer film, including molecular dopants.<sup>[47]</sup> The key requirement is that the molecule to be infiltrated must be soluble at sufficient concentration in a solvent that optimally swells but does not dissolve the polymer film. Although this requirement may appear challenging, we have shown that solvent blends can be used to tune the Flory–Huggins  $\chi$  parameter to optimally swell any conjugated polymer film.<sup>[57]</sup> Moreover, because it relies on swelling, which minimally affects the more crystalline regions of conjugated polymer films, the SqP method preserves the relative degree of crystallinity, crystalline domain orientation, and quality of an originally-cast polymer film even after infiltration of a molecule or a molecular dopant.<sup>[58–61]</sup>

In this work, we take advantage of the fact that SqP preserves the crystallinity and crystalline domain orientation in conjugated polymer films to study the electrical properties of a single semiconducting polymer doped with F<sub>4</sub>TCNQ as the crystallinity and chain morphology are systematically varied. We have chosen to focus our studies on the workhorse material poly(3-hexylthiophene-2,5-diyl) (P3HT), both because it allows us to compare directly to a large amount of previous work in the literature<sup>[11,12,17,19,25,26,29,33,36–38,40,42–47,49,50,62,63]</sup> and because the nature of this polymer allows the film crystallinity to be tuned relatively easily. We tune the crystallinity of P3HT in two different ways. First, we simply cast the original P3HT film from either a slowly or a rapidly evaporating solvent,<sup>[57,64]</sup> allowing direct control over the crystallinity of the originally cast film

and thus also over the doped film after SqP. Second, we take advantage of P3HT produced by a synthetic method that yields essentially 100% regioregular material,<sup>[65]</sup> providing additional enhancement of the crystallinity of both the original and doped films created by SqP.<sup>[58,66]</sup> We characterize the film morphology in each case by 2D grazing-incidence wide-angle X-ray scattering (GIWAXS), and in conjunction with theoretical modeling of the observed polaron spectrum, argue that the dopant does not  $\pi$ -stack within the polymer crystallites, but instead resides mainly in the films' amorphous regions and in the lamellae of the P3HT crystallites. Moreover, all of our SqP-produced films are of high enough quality that we can make conductivity and AC Hall effect measurements using electrodes spaced more than 1 cm apart. We find that the conductivity of the doped films is directly correlated to the crystallinity and crystallite domain orientation in the doped films. Despite having similar doping levels, the films with the most anisotropic edge-on orientation and overall highest degree of crystallinity show large improvements in mobility over more isotropic, amorphous films. The increased mobility comes directly from the doped carriers being able to delocalize more along the polymer chain in the more ordered systems, as reflected in AC Hall effect, temperature-dependent conductivity and optical absorption measurements, as well as theoretical modeling.

## 2. Results and Discussion

### 2.1. Controlling the Crystallinity of Molecularly Doped Conjugated Polymer Films

#### 2.1.1. Tuning the Morphology of Initially Cast and SqP-Doped P3HT Films

As mentioned above, the goal of this study is to systematically control the crystallinity of a single conjugated polymer, in this case P3HT, to understand the relationship between morphology, conductivity, and carrier mobility when the films are molecularly doped with F<sub>4</sub>TCNQ. To modify the crystallinity of our doped P3HT films, we start by simply spin-casting films of commercially purchased P3HT (Rieke metals,  $M_n = 55 \text{ kg mol}^{-1}$ , polydispersity  $\mathcal{D} = 2.4$ , regioregularity (RR) 93%) from two different solvents. It is well known that changing the solvent evaporation kinetics provides an effective way to manipulate the kinetics of conjugated polymer thin film formation, resulting in some control over the final morphology of the films.<sup>[64,67,68]</sup> Thus, to produce highly amorphous P3HT films with relatively little degree of crystallinity, we spin-coated the films at 1000 rpm for 60 s from a 1% w/v solution in chloroform (CF), which is a relatively fast-drying solvent. To generate films with higher degrees of crystalline content, we spin-coated P3HT at 1160 rpm for 20 s from a 2% solution in the relatively slow-drying solvent, *o*-dichlorobenzene (ODCB), allowing us to place the still-wet films in a closed Petri dish until dry, which effectively “solvent anneals” them.<sup>[68]</sup> Because we use the same batch of polymer for both film casting conditions, any chemical defects (e.g., fraction of oxidized segments along the polymer backbone, unexpected chemical species associated with the chain ends or catalyst/other materials leftover

from the polymer synthesis, differences in molecular weight, or regioregularity) that might affect the physics of the doped carriers are the same for both sets of films. Thus, because the SqP process allows us to dope these films and preserve their relative degree of crystallinity, any differences we observe in the doped films' conduction behavior must arise from differences in morphology and not from differences in chemistry.

Because commercial P3HT has only a relatively modest regioregularity, we are limited in the degree of crystallinity we can produce in spin-cast films of the commercial material.<sup>[60]</sup> Thus, to explore what happens when P3HT is made highly crystalline, we also worked with an in-house synthesized batch of P3HT that is essentially perfectly regioregular (100% RR P3HT;  $M_n = 17.5 \text{ kg mol}^{-1}$ ,  $\bar{D} = 1.09$ ).<sup>[65]</sup> The increased regioregularity produces significantly less disorder in spin-cast films, increasing the overall degree of crystallinity,<sup>[66]</sup> even after the films have been infiltrated by small molecules using SqP.<sup>[58]</sup> Because the polymer was produced via a different synthesis route, it is possible that compared to the commercial P3HT, the 100% RR material has different types and/or amounts of intrinsic chemical defects. At high doping levels, however, the properties of the doped material are dominated by the explicitly introduced doped polarons, so we believe that it is still legitimate to use this material as a means to understand the relationship between film morphology and the electrical behavior of the charge carriers. We used the same procedure to cast 100% RR P3HT films as we did for films of the commercial material cast from ODCB, with the exception of heating the 100% RR P3HT solution to 60 °C and casting it while hot in order to fully dissolve the material. The difference in film structure between the commercial material and the 100% RR material is apparent on the macroscale, where optical microscopy shows clear aggregates of crystallites with aggregate sizes on the order of tens of micrometers for the 100% RR P3HT films (see the Supporting Information for optical micrographs and additional details).

Once the initial P3HT films were prepared, we then doped the films using the SqP method by spin-coating solutions of 1 mg mL<sup>-1</sup> F<sub>4</sub>TCNQ in dichloromethane (DCM) on top of the P3HT films at 4000 rpm for 10 s. For all of our pristine and F<sub>4</sub>TCNQ-doped P3HT samples, as discussed further below, we characterized the nanoscale structure of the films by GIWAXS, UV-vis absorption and Fourier-transform infrared (FTIR) spectroscopy, and ellipsometric porosimetry to directly measure swelling of the polymer films by the solvent.

### 2.1.2. Characterizing Crystallinity and Crystalline Orientation Pristine and SqP-Doped P3HT Films

In order to determine the relative crystallinity, average crystallite size, and domain orientation in our pristine and doped P3HT films, we performed a series of 2D GIWAXS measurements, details of which are described in the Supporting Information. P3HT crystallites are well known to prefer an edge-on orientation of the chains. In this geometry, the  $\pi$ - $\pi$  stacking or (010) diffraction peak is observed predominantly in the in-plane direction and the lamellar or (100) diffraction peak, which corresponds to interchain stacking along the direction of the side chains, is observed predominantly in the out-of-plane

direction.<sup>[69,70]</sup> Charge carriers in conjugated polymer films move most freely along the conjugated polymer backbone, but for 2D and 3D transport, the carriers eventually need to hop between chains. The barrier for hopping between chains in the  $\pi$ -stacking direction is much lower than between chain backbones along the lamellar direction, which involves carrier motion through the side chains, so that charge transport in-plane is more facile than out-of-plane in the case of P3HT. In addition, crystalline regions of the film are expected to be more conductive than amorphous regions because of increased  $\pi$ -stacking in the crystalline regions. This is why it is important to understand and control the degree of crystallinity and the crystalline orientation within a doped polymer film. Since SqP largely preserves both the degree of crystallinity and the domain orientation,<sup>[58-60]</sup> it provides an excellent route to preparing molecularly doped P3HT films with controlled crystallinity.<sup>[47]</sup>

The 2D GIWAXS diffraction data in **Figure 1** provide information on the trends in relative crystallinity, polymer orientation, and typical crystallite size (or more formally, scattering coherence length) in the various pristine and doped P3HT films, as summarized in **Table 1**. For the pristine P3HT films, based on the integrated (100) peak area, there is a clear trend in relative crystallinity with the CF-cast film being the least crystalline, the ODCB-cast film being more crystalline, and the 100% RR P3HT film having the highest degree of crystallinity. **Figure 1 (a)** also shows that there is relatively little out-of-plane scattering for the (010) peak near 1.6 Å<sup>-1</sup> in all three films, consistent with a predominantly edge-on orientation of the P3HT crystallites. The inset shows that the 100% RR material, which has the highest degree of crystallinity, also has the lowest out-of-plane (010) scattering, indicative of an even greater preference for edge-on orientation for the crystallites in this film. The general trend is clearly that the more crystalline the film, the more edge-on oriented are the crystallites. These trends are consistent with those seen in previous work using these same materials in BHJ solar cells.<sup>[58]</sup>

After doping via SqP using a 1 mg mL<sup>-1</sup> solution of F<sub>4</sub>TCNQ in DCM, the GIWAXS data (solid curves) in **Figure 1** show that the (100) peaks shift to lower  $q$  (larger  $d$  spacing) and that the trend in both overall crystallinity and domain orientation seen in the pristine P3HT films is maintained through the SqP doping process, as expected.<sup>[47,48]</sup> Indeed, the doped 100% RR P3HT shows little in-plane (100) and out-of-plane (010) scattering, indicating that the high anisotropy of the edge-on oriented crystallites is maintained throughout the SqP doping process. Crystalline domain size, or more properly crystallite coherence length, calculated using the standard Scherrer equation, is also well-preserved in both the (100) and (010) directions upon doping (**Table 1**). Indeed, coherence length actually appears to increase slightly in the (100) direction upon doping, indicating that inclusion of F<sub>4</sub>TCNQ into the lattice does not disrupt the ability of the polymer chains to pack in a regular manner.

Perhaps the most striking change observed upon doping in all three processing conditions, however, is a splitting of the (010) peak; like the (100) peak, the original (010) shifts slightly to lower  $q$ , but a second  $\pi$ - $\pi$  stacking peak appears at higher  $q$ , around 1.8 Å<sup>-1</sup>. This new peak has also been seen in previous studies of P3HT doped with F<sub>4</sub>TCNQ,<sup>[38,46,71]</sup> and has

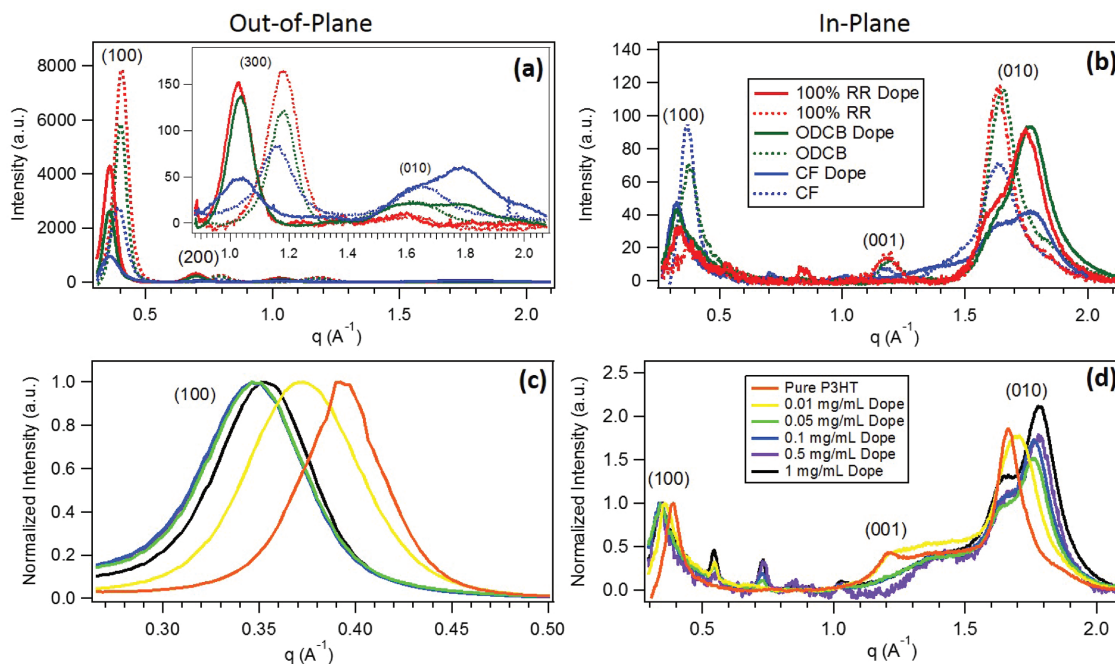


**Figure 1.** Integrated a) out-of-plane and b) in-plane X-ray diffraction patterns for chloroform (CF)-cast (blue dashed curves), *o*-dichlorobenzene (ODCB)-cast (green dashed curves), and 100% RR P3HT ODCB-cast polymer films (red dashed curves), as well as the same films after doping by SqP with 1 mg mL<sup>-1</sup> of F<sub>4</sub>TCNQ in dichloromethane (DCM; solid curves of the same colors, respectively). The inset in panel (a) shows the region around the P3HT out-of-plane (OOP) (010) peak on an expanded scale. The combination of in-plane and out-of-plane data for both the (100) and (010) diffraction can be used to conclude that for the pristine films, both the relative crystallinity and degree of edge-on crystallite orientation increase in the order CF-cast, ODCB-cast, 100% RR. Moreover, the data make clear that this order is maintained following doping with F<sub>4</sub>TCNQ by SqP. We also used GIWAXS to follow the doping process by examining films with progressively higher doping levels, as seen in integrated and normalized c) out-of-plane and d) in-plane X-ray diffraction peaks for P3HT films cast from ODCB at 1000 rpm for 60 s (red curves), followed by doping via SqP with different concentrations of F<sub>4</sub>TCNQ in DCM (various colored curves). Increasing doping levels causes a shift of the (100) diffraction peak to lower *q*, the appearance of a new (010) diffraction peak at higher *q*, and a complete loss of the (001) diffraction peak, indicative of the dopant residing in the lamellar regions of the sample but not the P3HT crystalline  $\pi$ -stacks, as suggested in Figure 2.

been attributed in the literature as evidence of  $\pi$ -stacking of P3HT:F<sub>4</sub>TCNQ co-crystallites and used to argue that F<sub>4</sub>TCNQ anions intercalate within the P3HT crystallite  $\pi$ -stacks.<sup>[38,50,71,72]</sup>

The argument that the new (010) peak at higher *q* in the doped films could be representative of the distance between the P3HT cation and F<sub>4</sub>TCNQ anion is based on the idea that the Coulomb attraction between the opposite charges pulls the two  $\pi$ -systems close together, decreasing their *d*-spacing; this

reasoning is loosely based on the idea that the anion stacks with the polymer  $\pi$ -system in much the same way as in charge transfer crystals, such as tetrathiafulvalene:TCNQ. This type of close contact, however, would lead to significant localization of the polarons on the P3HT chains which is not reflected in either our optical or electrical measurements, as discussed further below. Moreover, if  $\pi$ -stacked P3HT<sup>+</sup>:F<sub>4</sub>TCNQ<sup>-</sup> co-crystals did form in the doped films, this would lead to a doubling of

**Table 1.** Comparison of crystallinity (as determined by integrated out-of-plane peak area), orientation (out-of-plane (100)/(010) area ratio), crystallite coherence length (Å), volume fraction of pristine film swollen by saturated DCM vapor (%), exciton bandwidth (eV), and fraction aggregates (%) for pristine and doped CF-cast, ODCB-cast, and 100% RR P3HT films.

Film Property	CF-cast	ODCB-cast	100% RR P3HT	Doped CF-cast	Doped ODCB-cast	Doped 100% RR P3HT
Rel. OOP (100) peak area	1.0	2.0	2.5	0.5	2.0	3.0
Ratio of OOP (100)/(010)	37	230	506	36	253	481
(100) crystallite coherence length [Å]	75	96	86	92	105	103
(010) crystallite coherence length [Å]	38	50	52	29, 36	42, 48	45, 46
(100) <i>d</i> -spacing [Å]	16.0	15.6	15.5	17.8	17.5	17.5
(010) <i>d</i> -spacing [Å]	3.8	3.8	3.9	3.5, 3.9	3.6, 3.9	3.6, 3.9
% DCM in swollen film	11	9	7	–	–	–
Exciton bandwidth [eV]	0.135	0.11	0.044	–	–	–
%-aggregates	39	43	47	–	–	–

the unit cell size in the (010) direction. Figure 1b, however, clearly shows that there is no new peak near in the 0.8–0.9 Å<sup>-1</sup> range that would be reflective of a doubled unit cell.

Given these observations, combined with the fact that P3HT crystallites are known not to swell during SqP,<sup>[57]</sup> and the fact that there is little change in the integrated in-plane (010) scattering intensity upon doping, we find no reasonable mechanism for or evidence of F<sub>4</sub>TCNQ insertion into the P3HT  $\pi$ -stacks.<sup>[57]</sup> Indeed, the idea of  $\pi$ -stacked P3HT<sup>+</sup>:F<sub>4</sub>TCNQ<sup>-</sup> co-crystals being the dominant structure is not supported by the data presented here. Since the X-ray data presented here for P3HT doped with F<sub>4</sub>TCNQ by SqP are quite similar to that associated with doping by the traditional blend-casting method,<sup>[38,47]</sup> we believe that F<sub>4</sub>TCNQ anions do not intercalate into the P3HT crystalline  $\pi$ -stacks when doped by any method. Further support for this idea was recently offered by Hamidi-Sakr et al., who prepared films of sequentially processed F<sub>4</sub>TCNQ-doped P3HT where the polymer chains were aligned by rubbing, and found that the anion's absorption transition dipole was not parallel to that of the polaron, again suggesting that the anion does not  $\pi$ -stack in the P3HT crystallites.<sup>[48]</sup> Instead, when the P3HT crystallites are doped, the delocalization of the polaron among multiple adjacent chains slightly pulls the chains together, leading to the presence of the new peak at higher  $q$ . The fact that we see two peaks suggests that not every crystallite in the film is doped or fully doped, so that there are both neutral and charged crystalline regions in the doped films with different  $\pi$ -stacking distances.

In addition, the data in Figure 1a and Table 1 show that there is a fairly significant loss in the out-of-plane (100) peak scattering intensity upon doping. When the polymer films swell during SqP, it is primarily the amorphous regions of the film that swell,<sup>[57]</sup> but apparently the films can also swell slightly in the lamellar direction. This swelling provides a route for F<sub>4</sub>TCNQ to infiltrate between the P3HT side chains in the crystallites, increasing the lamellar spacing and causing both the observed shift of the (100) peak to lower  $q$  and the decrease in scattering intensity due to intercalation-induced disorder.

To better understand the process of F<sub>4</sub>TCNQ intercalation into P3HT films, we measured 2D GIWAXS on P3HT films SqP doped using a wide range of F<sub>4</sub>TCNQ concentrations in DCM. Figure 1c shows the region of the out-of-plane (100) peak on an enlarged scale. This panel reveals that the (100) peak shifts to lower  $q$  even at our lowest measured dopant concentration of 0.01 mg mL<sup>-1</sup> F<sub>4</sub>TCNQ, and further shifts to even lower  $q$  when the dopant concentration was increased to 0.05 mg mL<sup>-1</sup>.<sup>[48]</sup> Higher dopant concentrations than this do not further shift the (100) peak position, even though they continue to change the optical and electrical properties of the films. Similarly, the  $\pi$ -stacking (010) peak shows concentration-dependent changes at the same low dopant concentrations but remains relatively fixed past 0.05 mg mL<sup>-1</sup> doping concentration. Figure 1d shows that relative to pure P3HT, the 0.01 mg mL<sup>-1</sup> doped in-plane (010) peak appears broadened and shifted to higher  $q$ . By 0.05 mg mL<sup>-1</sup>, the (010) peak becomes clearly distinguishable as two different peaks, one at roughly the same  $q$  as the undoped P3HT (010) and one at higher  $q$ . The fact that the peak shifts happen only at low doping concentrations suggests that only a modest amount of F<sub>4</sub>TCNQ can penetrate into the

crystalline lamellae. Once the crystalline lamellar regions are as "filled" as possible, the rest of the dopant presumably resides in the amorphous regions of the sample. Since the amorphous regions are not visible by X-ray scattering, we see no further changes in the films' crystalline structure via GIWAXS.

In addition to the changes in the (100) and (010) peaks, the data in Figure 1b,d also show that the (001) peak near 1.2 Å<sup>-1</sup>, which is reflective of monomer-to-monomer registry along the P3HT backbone, exists in the pristine films but completely disappears upon molecular doping at concentrations  $\geq 0.05$  mg mL<sup>-1</sup> F<sub>4</sub>TCNQ. This indicates that doping by F<sub>4</sub>TCNQ causes a lateral shift of the polymer chains relative to each other in the P3HT crystallites, leading to a loss of registry in the along-the-chain direction. One possible cause for this shift could be reorganization of the optimal polymer backbone conformation upon doping.

When we combine this observation with the fact that the (100) peak shifts to lower  $q$  upon doping, we can construct a picture of how F<sub>4</sub>TCNQ infiltrates the different P3HT films, which is consistent with the data. Swelling during SqP allows some dopant molecules to enter the lamellar regions of the P3HT crystallites at low doping concentrations.<sup>[48]</sup> This increases the lamellar  $d$  spacing and potentially also changes the angle of the side chains relative to the polymer backbone. Changing the side-chain angle would cause a concomitant registry shift along the backbone, as illustrated in **Figure 2**, which could also explain the observed loss of the (001) peak. The polarons created by doping prefer to delocalize in the aromatic regions of the polymer, leading to an attraction between the polymer chains in the  $\pi$ -stacking direction and thus the observed new (010) peak. There is no structural evidence that F<sub>4</sub>TCNQ anions can  $\pi$ -stack with the crystalline polymer, so any anions that cannot fit in the side-chain regions of the polymer crystallites must sit in the amorphous regions of the films. In Section 2.2.1, we also will argue on the basis of theoretical modeling of the observed optical spectra that on average, the anions must sit at a distance of at least 0.6–0.8 nm from the polarons, which is also consistent with anions sitting in the lamellae or in the amorphous regions outside of the crystallites where the polarons reside.

### 2.1.3. The Swellability of Pristine P3HT Films with Different Degrees of Crystallinity

The SqP method relies heavily on the ability of the solvent in the second casting step to swell (but not dissolve) the underlying polymer. Perhaps not surprisingly, the differences in crystallinity between the different P3HT films that we observed via GIWAXS also affect the films' swellability; since amorphous polymer domains are the easiest to swell, the more crystalline a film is, the less ability it has to absorb solvent and increase its volume.<sup>[57]</sup> In order to measure swellability, we used spectroscopic ellipsometry to measure the optical properties ( $n$  and  $k$ ) of the different crystallinity polymer films both as-cast and after being exposed to the saturated vapor of the secondary casting solvent, DCM. Using the ellipsometric data in conjunction with the effective medium approximation, we were able to quantify the volume fraction of polymer and solvent in the

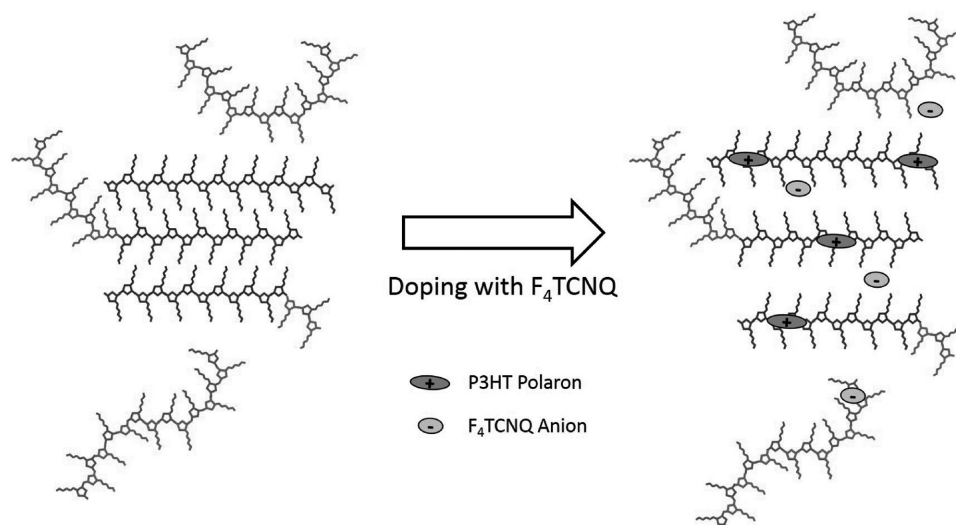


**Figure 2.** Cartoon consistent with the GIWAXS data illustrating how  $F_4TCNQ$  anions could incorporate into the lamellar regions of the crystallites as well as the amorphous regions of the film. The presence of the anion causes the side chains to shift in order to incorporate the new  $F_4TCNQ$  volume, which, in turn, causes the increase in spacing in the lamellar direction and the loss of along-the-chain registry. Polarons can also delocalize between chains in the  $\pi$ -stacking direction, leading to a decrease in the  $\pi$ - $\pi$  stacking distance (not shown).

swollen film;<sup>[57]</sup> a more detailed explanation of this procedure is included in the Supporting Information, and the experimental results are summarized in Table 1. Not surprisingly, the CF-cast film shows the greatest ability to swell, taking up 11% by volume DCM, followed by 9% DCM for the ODCB-cast film, and only 7% DCM for the 100% RR P3HT. This follows the expected trend of less swelling with higher-crystalline films, in good agreement with the GIWAXS data, discussed above.

Although the swelling trend is as expected, the swelling data are important in their own right because the ability to dope the films depends directly on their swellability; infiltration of  $F_4TCNQ$  via SqP depends directly on the degree of swelling. We note that it has been argued in the literature that it is easier to dope more crystalline P3HT because the more crystalline the polymer is, the more delocalized and thus the more stable the polarons become.<sup>[45,73]</sup> Thus, when doping P3HT by SqP, we anticipate a trade-off with polymer crystallinity; it becomes harder to infiltrate molecules by SqP into more crystalline polymer films,<sup>[58]</sup> but the molecules that do infiltrate should be able to dope the polymer more effectively, as discussed further below.

## 2.2. The Optical and Electrical properties of Sequentially Processed Controlled-Crystallinity $F_4TCNQ$ -Doped P3HT Films

### 2.2.1. The Spectroscopy of Controlled-Crystallinity SqP-Doped P3HT Films

We now shift our focus to the optical properties of our sequentially processed  $F_4TCNQ$ -doped P3HT films. **Figure 3a** shows the absorption spectra of the three different pristine P3HT films prior to doping via SqP. The redshift of the main exciton absorption band and increase in vibronic structure seen in the 100% RR film relative to the ODCB- and CF-cast films are a direct reflection of increased crystalline order. The absorption

of the films with different degrees of crystallinity can be quantitatively analyzed using a theoretical model that has been described previously;<sup>[74,75]</sup> details of our application of the model to these spectra are given in the Supporting Information, and the results are summarized in Table 1. The general trend shows decreasing exciton bandwidth and an increasing percentage of crystalline aggregates, in the order CF-cast < ODCB-cast < 100%-RR. These results directly support the conclusions we reached via GIWAXS, which show that the CF-cast film is the most amorphous, followed by the ODCB-cast film, with the 100% RR P3HT having the largest amount of crystalline order.

In addition to changes in the spectrum of P3HT excitons with polymer structure, it is also known that polarons become increasingly delocalized as the effective conjugation length is increased.<sup>[76]</sup> Our ability to tune the degree of order/crystallinity of our SqP-doped films provides a new route to cleanly examine this relationship. **Figure 3b** shows the absorption spectra of the same P3HT films in panel (a) after doping by SqP with 1 mg mL<sup>-1</sup>  $F_4TCNQ$  in DCM; the doped spectra are normalized to the intensity of the mid-IR peak near 0.5 eV for ease of comparison. The data show clearly that upon doping, the neutral P3HT exciton absorption between 2.0 and 2.75 eV is decreased in all three films, and that a new feature appears near 3.0 eV, corresponding to absorption by both the neutral and anionic forms of  $F_4TCNQ$ . There is also new absorption in the 1.3–1.8 eV region, corresponding to the P2 absorption band of the P3HT polaron,<sup>[17,37,42,77]</sup> which unfortunately also overlaps an additional absorption band of the  $F_4TCNQ$  anion (which is responsible for the observed vibronic peaks in this region).<sup>[37,47,78]</sup>

Since the data in **Figure 3b** are normalized to the peaks of the P1 bands, it is clear that for the same intensity of P1 polaron absorption, the intensities of the P2/ $F_4TCNQ^-$  and depleted neutral P3HT absorptions are not the same for the three films with different crystallinities, even though the three films were

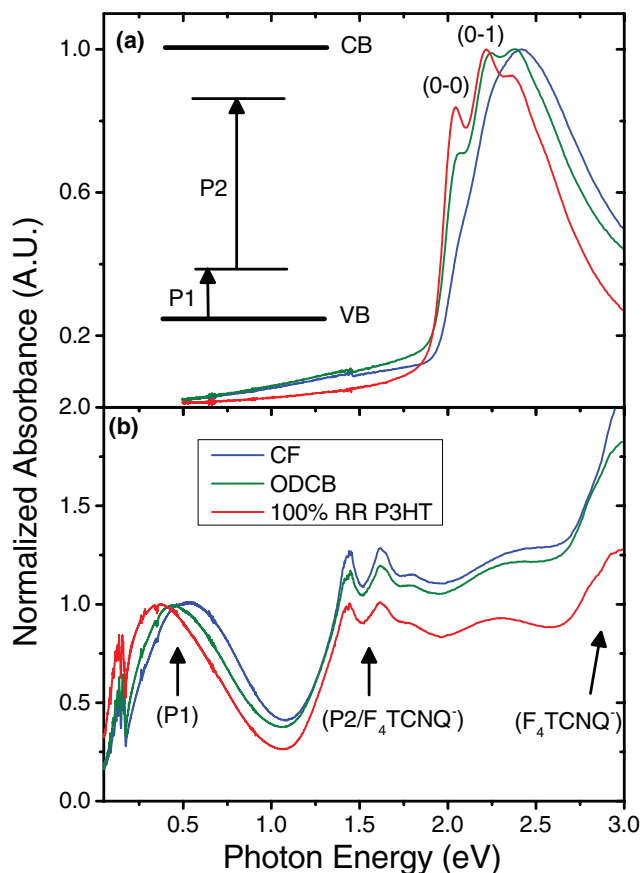


**Figure 3.** a) UV-vis absorption data for pristine CF-cast P3HT (blue curve), ODCB-cast P3HT (green curve), and 100% RR P3HT (red curve) films. b) Combined FTIR (0.05–0.5 eV) and UV-vis (0.5–3.0 eV) absorption spectra for the same P3HT films after doping via SqP with 1 mg mL<sup>-1</sup> F<sub>4</sub>TCNQ in DCM. The data are normalized to the peak intensity of the P1 absorption band in the 0.3–0.5 eV region. Clearly, the polaron P1 band redshifts, the relative absorption intensity below 0.18 eV increases, and the overall P1 absorption cross section increases with increasing polymer crystallinity. The inset in panel (a) shows a representative energy level diagram for the P1 and P2 transitions of the polaron.

doped by SqP with the same 1 mg mL<sup>-1</sup> F<sub>4</sub>TCNQ solution. Instead, relative to the P1 band absorption intensity, the more crystalline films have a greater depletion of the neutral P3HT exciton absorption, as well as a lower P2/F<sub>4</sub>TCNQ<sup>-</sup> absorption. The fact that the P1, P2, and depleted exciton peaks do not have the same ratio strongly suggests that either the cross section of the P1 absorption is sensitive to the film crystallinity, or that the films have different numbers of trapped and free polarons, which may have similar absorption spectra but different absorption cross sections. It is also possible that the absorption cross section of the F<sub>4</sub>TCNQ anion may be different in different crystalline environments. Indeed, despite great effort, it has proven difficult to pin down the cross section of the anion in a solid film environment, where it is at least an order of magnitude different from that in solution.<sup>[47]</sup> Unfortunately, the uncertainties of the cross sections of the anion, trapped P3HT polarons, and free P3HT polarons with different degrees of delocalization mean that it is not possible to rely solely on optical means to quantify carrier densities in P3HT that is highly doped with

F<sub>4</sub>TCNQ. This is why we rely on AC Hall effect measurements to determine the free carrier concentration, as discussed further below.

Figure 4a shows the P1 polaron absorption band for all three films on an expanded scale. Clearly, the P1 peak redshifts with increasing crystallinity of the doped P3HT film, from 0.55 eV for the CF-cast to 0.35 eV for the 100% RR P3HT, indicating greater delocalization of the polaron in the more crystalline material.<sup>[76]</sup> The structure seen in the region below 0.18 eV is due to P3HT vibrations (so-called infrared IR-active vibrations, or IRAVs); overtones of the IRAVs as well as absorption from atmospheric water and CO<sub>2</sub> are responsible for the small peaks superimposed on the main band at higher energies. This figure also makes clear that the IRAV portion of the absorption spectrum below 0.18 eV increases in intensity relative to the main band as the crystallinity of the polymer increases. The absorption spectrum of doped P3HT has been simulated in recent theoretical work,<sup>[79,80]</sup> with the lower energy IRAV-structured band arising mainly from interchain transitions in more ordered polymers but becoming dominated by intrachain transitions in more disordered material. The simulations accurately predicted the spectrum of P3HT doped by charge modulation,<sup>[79]</sup> when no anions were present (cf., red dashed curve in Figure 4b).

By comparison to the previous simulations of doping by charge modulation,<sup>[79]</sup> the P1 absorptions of our F<sub>4</sub>TCNQ-doped P3HT samples show considerable Gaussian broadening, which must be due to the presence of the anions. Figure 4b shows simulated IR spectra for P3HT using the same theoretical model from Ghosh et al.,<sup>[79]</sup> but with the addition of a negative point charge to account for the presence of the anion. The point charge was located in several different regions inside and at the edge of the simulated P3HT crystallites, but the results depended more on the distance of the point charge from the polaron than the direction; see the Supporting Information for details. As discussed in the Supporting Information, the choice of dielectric constant used in the calculation to account for screening of the polaron–anion Coulomb interaction is important to simulating our experimental P1 absorption spectra. We chose a distance-dependent dielectric constant<sup>[81]</sup> that we believe makes the most physical sense for our system, details of which are in the Supporting Information. The results of the calculations are shown in Figure 4b, which indicate that proximity of the anion dramatically changes the location, shape, and cross section of the P1 absorption peak. Close proximity ( $\leq 4$  Å) severely localizes the polaron to the region of the anion, leading to a large blueshift and narrowing of the main P1 peak and lowering of the IRAV portion of the peak at low energy (blue curve) relative to the simulated band with the anion at infinite distance (red dashed curve). As the anion is moved farther from the polaron, the polaron delocalizes, leading to a redshift and broadening of the intrachain peak, and a relative increase in the intensity of the low-energy intramolecular IRAV peak (light blue, green, yellow, and orange curves). These calculations also show that as the polaron localizes, the total absorption cross section of the P1 band decreases, further emphasizing the difficulty in using absorption spectra to extract accurate carrier concentrations.

The broadened and redshifted experimental intrachain absorption that we see for the polarons in Figure 4a, along with

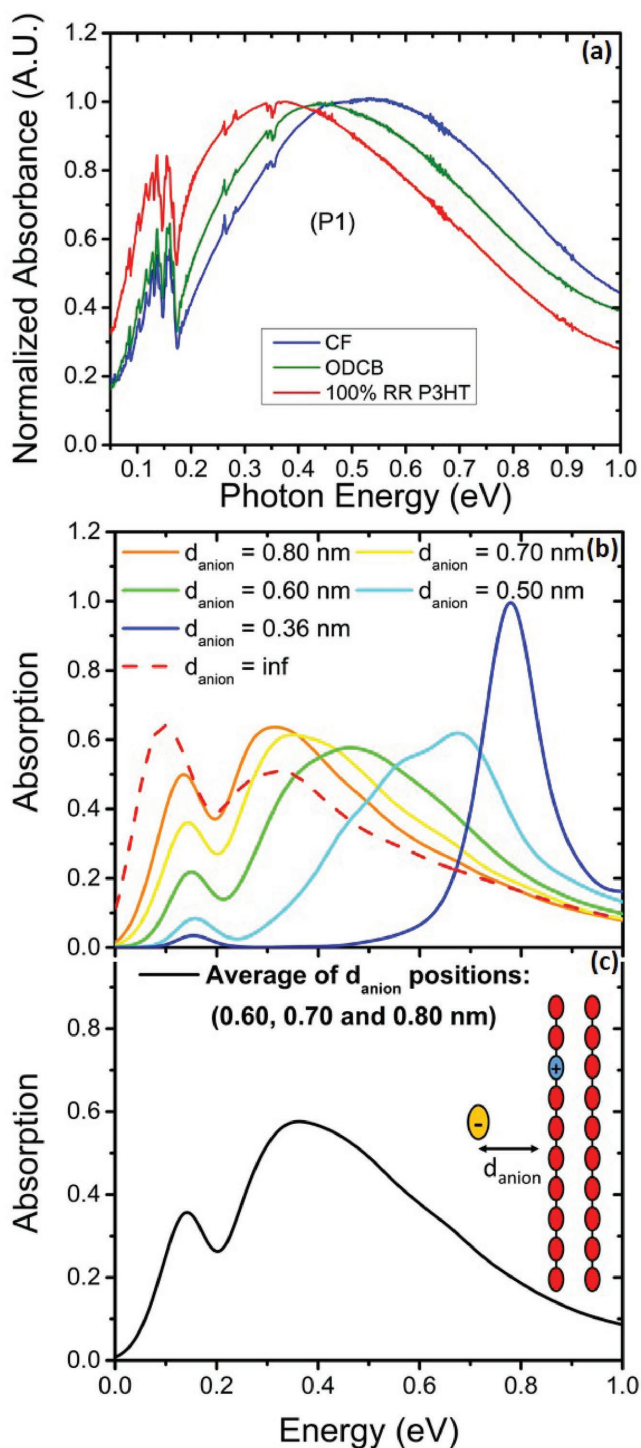


**Figure 4.** a) Experimental absorption spectra of the P1 polaron transition for CF-cast (blue curve), ODCB-cast (green curve), and 100% RR (red curve) P3HT doped via SqP with  $1 \text{ mg mL}^{-1}$   $F_4\text{TCNQ}$  in DCM. b) Simulated P1 absorption band with a negative point charge representing the anion placed 0.36 nm (blue curve), 0.5 nm (light blue curve), 0.6 nm (green curve), 0.7 nm (yellow curve), 0.8 nm (orange curve), and infinitely far away (red dashed curve) from a  $10 \times 2$  P3HT chain array. Spectra were obtained by averaging over 1000 configurations of random site disorder; see the Supporting Information. c) Simulated P1 absorption band obtained by further averaging over different anion distances

the fact that the intensity of the IRAV portion of the band is at least half that of the intrachain band, strongly suggests that the polarons in our samples are not localized immediately next to anions. This is consistent with our conclusions from the GIWAXS data that suggested that the  $F_4\text{TCNQ}$  anions lie in either the P3HT lamellae or in the amorphous regions near the P3HT crystallites, and do not form  $\pi$ -stacked co-crystals with the polymer (distance  $\approx 3.5 \text{ \AA}$ ).<sup>[48]</sup> We conclude that while there may be some small contributions to the spectrum from anions at the  $\pi$ -stacking distance from the polaron in the amorphous regions, which serve to increase the broadening of the P1 absorption spectral envelope,  $\pi$ -stacking does not appear to be the dominant structural motif to accommodate the  $F_4\text{TCNQ}$  in our SqP-doped samples.

Figure 4c shows a simulated polaron spectrum constructed by averaging over 1000 different configurations of random site disorder (see the Supporting Information) and anion distances in the range 0.6–0.8 nm from the polymer backbone, which gives good general agreement with both the spectral shape and the peak position of our measured spectra in Figure 4a. Interestingly, in order to reproduce the peak position in the measured IR absorption spectrum near 0.35 eV for 100% RR P3HT, the anion must be at least 0.5 nm from the stack, with the exact value depending on the dielectric constant chosen for the simulations (see the Supporting Information). This again points to the idea that in such well-ordered crystals with minimal amorphous regions,  $\pi$ -stacking of the anion with the polymer is not permitted. In less-ordered samples, some  $\pi$ -stacking may occur in the amorphous regions. The more disordered  $\pi$ -stacks in the amorphous regions may contribute to the width of the polaron absorption band, but they are not visible by GIWAXS. The idea that the polarons in our samples are delocalized is also consistent with the mobilities we extract from our electrical measurements, described below, which are comparable to those seen in doped samples without anions present.<sup>[82–87]</sup>

Given the results of the modeling in Figure 4b,c, the redshift we see of the intrachain polaron band with increasing P3HT crystallinity has two possible origins: the band could redshift because the polarons are more intrinsically delocalized in more crystalline films<sup>[76]</sup> or the band could redshift because the polarons are farther, on average, from the anions, so there is less anion-induced localization in more crystalline films. Table 1 shows that although the average size of the P3HT crystallites increases from the CF-cast to 100% RR P3HT films, our simulations suggest that the size change alone is not enough to account for the shift of the intrachain P1 peaks: the average crystallite size simply does not change enough to cause a significant change in  $d_{\text{anion}}$  (presuming that the anions are located outside the crystallites). Films with an increased fraction of amorphous regions, however, could possibly have  $F_4\text{TCNQ}$  anions located in disordered  $\pi$ -stacks, placing them closer to

ranging from 0.6 to 0.8 nm, giving good general agreement with the spectral shape and peak position seen experimentally in panel (a). The inset in panel (c) is a cartoon representation of the simulation. The fact that the experimental spectra are not strongly blueshifted or narrowed suggests that anions do not lie within  $5 \text{ \AA}$  of the polymer, reinforcing the conclusion that the  $F_4\text{TCNQ}$  anion does not  $\pi$ -stack with crystalline P3HT.

the location of the polaron than in the crystallites. Thus, we believe that it is a combination of both increased intrinsic delocalization and decreased localization from the anion that leads to the more redshifted polaron absorption in the more crystalline films.

### 2.2.2. AC Hall Effect Measurements on Controlled-Crystallinity SqP-Doped P3HT Films

With the optical and structural properties of the doped films characterized, we turn in this section to correlating the controlled crystallinity of the SqP-doped films with their electrical properties. We examined the conductivities of all three of our P3HT films SqP doped with 1 mg mL<sup>-1</sup> F<sub>4</sub>TCNQ in DCM using both collinear four-point probe (2.5 mm spacing between electrodes) and van der Pauw measurements (electrodes at the corners of a 1.5 × 1.5 cm square),<sup>[88]</sup> and found that as in our previous work,<sup>[47]</sup> the two methods always gave conductivities that agreed to within a few percent. At room temperature, we find that the conductivity of the doped CF-cast P3HT film is only 2.1 S cm<sup>-1</sup>, but that increasing the crystallinity by casting the film from ODCB yields a conductivity of 5.7 S cm<sup>-1</sup>, with a further increase to ≥10 S cm<sup>-1</sup> for the 100% RR P3HT (see the Supporting Information); our highest measured conductivity for the 100% RR material reached 12 S cm<sup>-1</sup>, effectively an order of magnitude higher than what is typically reported for P3HT films doped with F<sub>4</sub>TCNQ by traditional blend-casting methods.<sup>[11,37,38]</sup>

The improvement in conductivity that we observe with the SqP method leads to an important question: since the conductivity  $\sigma$  varies as the product of carrier concentration  $n$  and mobility  $\mu$  according to  $\sigma = nq\mu$ , where  $q$  is the fundamental unit of charge, does the improved conductivity result from an increased number of carriers, increased polaron mobility, or some combination of the two? To answer this question, we employed AC magnetic field Hall effect measurements. This relatively new technique has been shown previously to give reliable results for low-mobility materials, which typically have Hall voltages too small to accurately distinguish from the noise present in DC Hall measurement techniques.<sup>[89–91]</sup>

It is important to note that although the AC Field Hall technique is reliable, the interpretation of the data for low-mobility materials with hopping-dominated carrier transport is not entirely straightforward. In traditional measurements, the Hall voltage,  $V_H$ , provides a measure of the potential created by the Lorentz force acting to bend charges with band-like transport around a magnetic field:  $V_H = IB/nq$ , where  $I$  is the magnitude of the sourced current and  $B$  is the value of the applied magnetic field.<sup>[89]</sup> Carriers that move by hopping, however, are not influenced by the magnetic field in the same way as band-like carriers, effectively screening the applied magnetic field. This can lead to smaller measured  $V_H$  values, which in turn can affect estimates of the carrier concentration (and via the measured conductivity, also affect estimates of the carrier mobility), as has been discussed in detail in recent work by Podzorov and co-workers.<sup>[92]</sup> Even if the largest AC Hall mobilities we measure for the doped 100% RR P3HT underestimate the actual mobility, it is worth noting that all of our values are in

**Table 2.** Comparison of carrier density ( $n$ ), mobility ( $\mu$ ), and conductivity ( $\sigma$ ) measured by the AC magnetic field Hall effect technique for F<sub>4</sub>TCNQ-doped P3HT samples by SqP.

Crystalline Morphology	$n$ [cm <sup>-3</sup> ]	$\mu$ [cm <sup>2</sup> V <sup>-1</sup> s <sup>-1</sup> ]	$\sigma$ [S cm <sup>-1</sup> ]
CF-cast	$5.9 \times 10^{20}$	0.02	1.4
ODCB-cast	$7.1 \times 10^{20}$	0.05	5.7
100% RR P3HT	$4.9 \times 10^{20}$	0.12	9.1

the general range of those determined previously by field-effect transistor (FET) and DC Hall effect measurements for doped P3HT.<sup>[93]</sup>

Given these issues with the interpretation of Hall data in low-mobility molecularly doped conjugated polymers, for this study we focus on qualitative trends presented by the data, rather than the exact quantitative values, to gain insights into the effects of controlling crystallinity on the charge transport properties of our doped samples. **Table 2** summarizes the results of AC magnetic field Hall effect measurements on our various SqP-doped P3HT films; in the values we report, we calculate the carrier concentration using the traditional Hall coefficient equations, which assume band-like transport. We note that the trends we report are valid as long as the three samples have roughly equivalent amounts of screening of the applied  $B$  field, and we expect that this screening leads to a slight overestimate of the reported carrier densities. The data show a clear trend of increasing Hall-based carrier mobility,  $\mu$ , with increasing crystallinity. In contrast, the carrier concentration  $n$  remains roughly constant as the crystallinity increases, so we can assign the large increase in conductivity as resulting from increasing carrier mobility with increasing film crystallinity. The slight decrease in carrier concentration for the 100% RR film could be the result of poorer intercalation of F<sub>4</sub>TCNQ due to decreased swelling, as discussed above. Moreover, the lower concentration in the 100% RR sample, along with the higher absorption intensity, emphasizes the idea that the polarons in more crystalline samples have a higher absorption cross section than those in less crystalline samples.

The measured increase in carrier mobility with increasing P3HT crystallinity likely results from a combination of the improvement in “intrinsic” mobility of the undoped polymer, which persists upon SqP doping, with less anion-induced localization of the polarons as the anions are, on average, slightly farther away in the more crystalline material. This idea that much of the mobility improvement comes from intrinsic polaron delocalization is in accord with measurements on gatedoped P3HT films in field-effect transistors that also observed that in-plane mobility increases with increased polymer crystallinity.<sup>[2,94]</sup> We note that increasing  $M_w$  of the polymer is also known to increase carrier mobility by allowing for better formation of tie chains between crystalline domains,<sup>[86,95]</sup> but this effect clearly plays no role in our data. This is because our highest observed mobility is in the 100% RR P3HT sample, which has a much lower degree of polymerization than the commercially available P3HT used for the CF- and ODCB-cast films. Clearly, the increase in the quantity and size of the crystalline regions reported in Table 1 is what is responsible for the observed mobility increase.

### 2.2.3. Temperature-Dependent Conductivity of Controlled-Crystallinity SqP-Doped P3HT Films

To better understand the nature of the carrier transport in our SqP-doped P3HT films with three different degrees of crystallinity, we measured the temperature dependence of the conductivity from 50 to 300 K (see the Supporting Information for details). The data demonstrate that all of our doped films exhibit classic disordered organic semiconductor behavior with a conductivity that increases with increasing temperature.<sup>[84]</sup> We investigated the specific charge transport mechanism for each film condition by fitting the data to several different theoretical models, which are discussed in more detail in the Supporting Information.

In order to best fit the experimental data to known models over the full temperature range measured, we followed the method in refs. [28] and [93] by performing logarithmic differentiation to linearize the temperature-dependent conductivity,  $\sigma \propto \exp[(-1/T)^x]$ , the results of which are shown in Figure 5. In general, the observed temperature dependence of our samples is in good agreement with other works that observed that the Mott variable-range-hopping (VRH) model described the temperature-dependent conductivity of doped conjugated polymers.<sup>[28,29,93,96]</sup> More specifically, the ODCB-cast and 100% RR P3HT films show a  $T$ -dependent conductivity that is well described by the Efros–Shklovskii (ES) VRH model<sup>[97]</sup> at low temperatures and by the more traditional Mott VRH model<sup>[98]</sup> at higher temperatures. ES VRH accounts for the Coulomb interaction, predicting conductivity with a characteristic temperature dependence of  $T^{-1/2}$ .<sup>[97]</sup> The Coulomb interaction can be neglected above a critical  $T$ , leading to the more traditional Mott VRH model, which predicts a temperature dependence of the conductivity that goes as  $T^{-1/4}$ . In contrast to those of the more crystalline films, the  $T$ -dependent conductivity of the doped CF-cast films fits best to an  $\approx T^{-1/3}$  dependence over the entire temperature range, indicating that the increased disorder in the CF-cast samples results in a different (hopping) conduction mechanism. For all of our samples, as we approach room temperature there is a drastic decrease in the  $T$ -dependence of the conductivity (marked by the arrows in Figure 5), indicating a regime that deviates from hopping-dominated transport and is approaching a more diffusive transport mechanism. These observations for our SqP-doped samples are consistent with previous results for electrochemically doped P3HT films with high carrier densities.<sup>[93]</sup>

Since all three of our doped samples with different crystallinities are roughly in this same transport regime at room temperature, it means that whatever the balance of band-like and hopping-based transport, all of our samples have approximately the same degree of screening of the applied magnetic field. This means that even if the absolute values of the mobilities we extract from the AC Hall measurements are underestimated, the degree of underestimation is likely similar for all three of our samples, allowing us to make meaningful relative mobility comparisons between the samples. Since the transition from hopping to diffusive transport starts at slightly lower temperatures with increasing polymer crystallinity, it is possible that further improvements in the crystallinity might actually bring about a complete transition to band-like transport at similar carrier concentrations at room temperature.

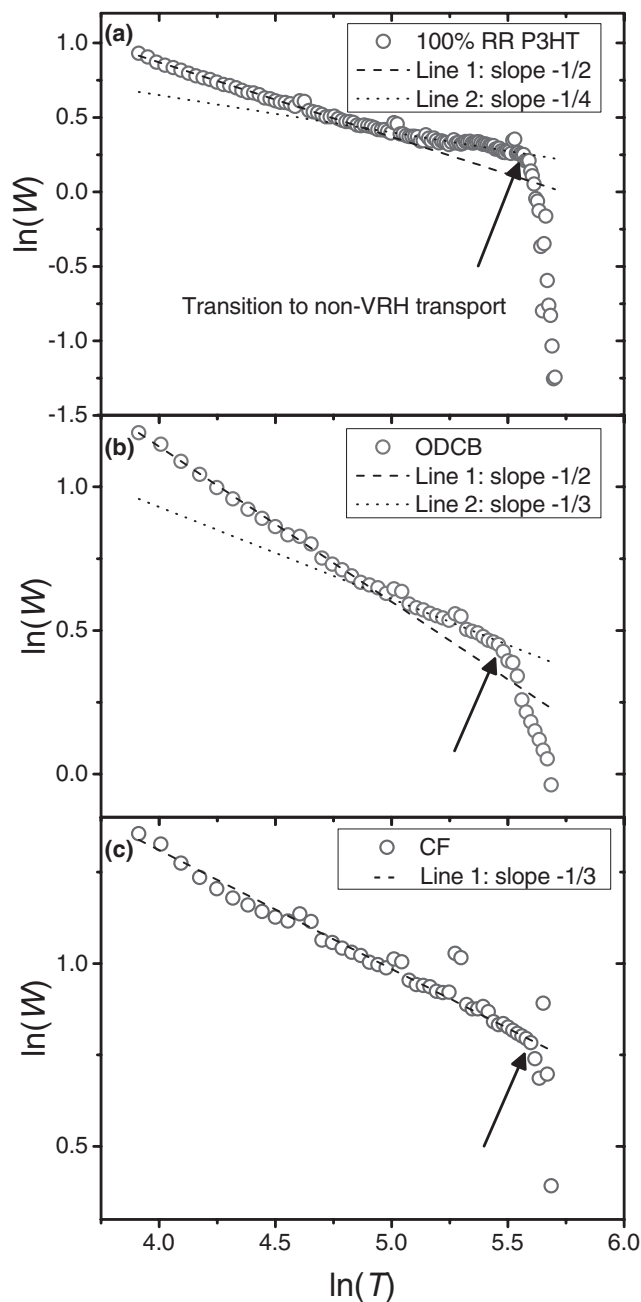


**Figure 5.** Logarithmic derivative plot of the conductivity of different P3HT films doped via SqP with  $1 \text{ mg mL}^{-1} \text{ F}_4\text{TCNQ}$  in DCM versus temperature: a) 100% RR P3HT, b) ODCB-cast, and c) CF-cast. The dashed and dotted lines are linear fits with the corresponding slopes listed in the legend. The arrows mark the temperature at which the behavior deviates from traditional variable-range-hopping transport.

### 3. Conclusions

We have shown that modifying the crystallinity of a conjugated polymer film prior to doping can lead to improved electrical properties after molecular doping, and we demonstrated this for the P3HT: $\text{F}_4\text{TCNQ}$  system by preserving the crystalline properties of pristine films by introducing the dopant via SqP. By changing the solvent used to cast P3HT films and by

synthetically improving the polymer regioregularity, we were able to prepare pristine P3HT films with three distinct degrees of crystallinity, as confirmed by GIWAXS, swelling measurements, and UV-vis spectroscopy. In addition to overall crystallinity, we also saw that the edge-on preferred crystalline domain orientation was enhanced in the more crystalline P3HT samples, and that both the degree of crystallinity and orientation could be maintained after doping with F<sub>4</sub>TCNQ via SqP. Our GIWAXS measurements showed that no matter what the overall degree of crystallinity is, doping led to an increase of the lamellar crystalline spacing, a decrease in the  $\pi$ -stack spacing, and a loss of registry in the along-the-chain direction. Together, these observations suggest that the F<sub>4</sub>TCNQ anions go first into the crystalline lamellar regions and then begin to incorporate into the polymer amorphous regions, but they do not  $\pi$ -stack in the polymer crystallites.

When we performed optical measurements of the doped P3HT films, we found redshifted absorption bands with higher cross sections that indicated greater delocalization of the polarons in the more crystalline films. Simulations of the polaron absorption spectra suggest that close contact between the anion and polaron (such as that would occur if the anions  $\pi$ -stacked in the polymer crystallites) would lead to localized polarons characterized by blueshifted and narrowed absorption bands with a lower cross section, which is not what we observed. Instead, the simulations are consistent with F<sub>4</sub>TCNQ anions residing, on average, between 6 and 8 Å from the polaron location, consistent with the GIWAXS assignment of the anions residing in the lamellar regions of the crystallites as well as the amorphous regions of the film.

The increased polaron delocalization upon increased P3HT crystallinity also leads to improved in-plane conductivity, reaching over 10 S cm<sup>-1</sup>, as verified by four-point probe measurements. AC field Hall effect measurements strongly suggest that the improved conductivity results directly from improved carrier mobility; the mobility increased by a factor of 5 from the most amorphous to the most crystalline sample. The improvement in mobility comes mostly in the form of increased charge carrier delocalization in the crystalline regions of the film, as well as decreased polaron localization caused by the proximity of F<sub>4</sub>TCNQ anions. Temperature-dependent conductivity measurements confirmed that the carrier transport at low temperatures takes place by variable-range hopping, with the beginning of a transition to a more diffusive transport mechanism taking place around room temperature. This transition was most apparent for the 100% RR P3HT film, alluding to the possibility that further structural engineering or material design could potentially allow reaching pure band-like conduction in molecularly doped semiconducting polymers at room temperature. Overall, the ability to independently modify the structure of a polymer film and then preserve that structure upon doping by SqP offers significant advantages for fabricating high-quality semiconducting polymer thin films for organic electronic devices.

## Supporting Information

Supporting Information is available from the Wiley Online Library or from the author.

## Acknowledgements

This work was supported by the National Science Foundation under grant numbers CBET-1510353 and CHE-1608957. Use of the Stanford Synchrotron Radiation Lightsource, SLAC National Accelerator Laboratory, was supported by the U.S. Department of Energy, Office of Science, Office of Basic Energy Sciences under Contract No. DE-AC02-76SF00515. F.C.S. was supported by the National Science Foundation, grant number DMR-1533954. Computations were supported by an NSF instrumentation grant, CNS-09-58854. C.K.L. also recognizes support from NSF grant numbers DMR-1533372 and DMR-1708317.

## Conflict of Interest

The authors declare no conflict of interest.

## Keywords

charge transport, doping, Hall Effect, morphology, semiconducting polymers

Received: May 17, 2017

Revised: August 4, 2017

Published online:

- [1] J. H. Burroughes, D. D. C. Bradley, A. R. Brown, R. N. Marks, K. Mackay, R. H. Friend, P. L. Burns, A. B. Holmes, *Nature* **1990**, *347*, 539.
- [2] H. Sirringhaus, *Science* **1998**, *280*, 1741.
- [3] E. Fukada, *1998 Proc. – IEEE Ultrason. Symp.* **2000**, *1*, 597.
- [4] G. Yu, J. Gao, J. C. Hummelen, F. Wudl, A. J. Heeger, *Science* **1995**, *270*, 1789.
- [5] S. Günes, H. Neugebauer, N. S. Sariciftci, *Chem. Rev.* **2007**, *107*, 1324.
- [6] Y. Liang, L. Yu, *Polym. Rev.* **2010**, *50*, 454.
- [7] O. Bubnova, X. Crispin, *Energy Environ. Sci.* **2012**, *5*, 9345.
- [8] Y. H. Kim, S. Hotta, A. J. Heeger, *Phys. Rev. B* **1987**, *36*, 7486.
- [9] M. Lögdlund, R. Lazzaroni, S. Stafström, W. R. Salaneck, J.-L. Brédas, *Phys. Rev. Lett.* **1989**, *63*, 1841.
- [10] E. F. Aziz, A. Vollmer, S. Eisebitt, W. Eberhardt, P. Pingel, D. Neher, N. Koch, *Adv. Mater.* **2007**, *19*, 3257.
- [11] K.-H. Yim, G. L. Whiting, C. E. Murphy, J. J. M. Halls, J. H. Burroughes, R. H. Friend, J.-S. Kim, *Adv. Mater.* **2008**, *20*, 3319.
- [12] C. Y. Kao, B. Lee, L. S. Wielunski, M. Heeney, I. McCulloch, E. Garfunkel, L. C. Feldman, V. Podzorov, *Adv. Funct. Mater.* **2009**, *19*, 1906.
- [13] B. Lüssem, C.-M. Keum, D. Kasemann, B. Naab, Z. Bao, K. Leo, *Chem. Rev.* **2016**, *116*, 13714.
- [14] Z. Q. Gao, B. X. Mi, G. Z. Xu, Y. Q. Wan, M. L. Gong, K. W. Cheah, C. H. Chen, *Chem. Commun.* **2008**, 117.
- [15] E. Alveroglu, *J. Mol. Struct.* **2015**, *1086*, 86.
- [16] J. Li, G. Zhang, D. M. Holm, I. E. Jacobs, B. Yin, P. Stroeve, M. Mascal, A. J. Moulé, *Chem. Mater.* **2015**, *27*, 5765.
- [17] J. Yamamoto, Y. Furukawa, *J. Phys. Chem. B* **2015**, *119*, 4788.
- [18] S. Qu, Q. Yao, W. Shi, L. Wang, L. Chen, *J. Electron. Mater.* **2016**, *45*, 1389.
- [19] V. A. Kolesov, C. Fuentes-Hernandez, W.-F. Chou, N. Aizawa, F. A. Larrain, M. Wang, A. Perrotta, S. Choi, S. Graham, G. C. Bazan, T.-Q. Nguyen, S. R. Marder, B. Kippelen, *Nat. Mater.* **2016**, *1*, 1.
- [20] A. Loiudice, A. Rizzo, M. Biasiucci, G. Gigli, *J. Phys. Chem. Lett.* **2012**, *3*, 1908.
- [21] X. Han, Z. Wu, B. Sun, *Org. Electron.* **2013**, *14*, 1116.

- [22] Y. Zhang, H. Zhou, J. Seifert, L. Ying, A. Mikhailovsky, A. J. Heeger, G. C. Bazan, T.-Q. Nguyen, *Adv. Mater.* **2013**, *25*, 7038.
- [23] H. Yan, J. G. Manion, M. Yuan, F. P. García de Arquer, G. R. McKeown, S. Beaupré, M. Leclerc, E. H. Sargent, D. S. Seferos, *Adv. Mater.* **2016**, *28*, 6491.
- [24] S. Yu, J. Frisch, A. Opitz, E. Cohen, M. Bendikov, N. Koch, I. Salzmann, *Appl. Phys. Lett.* **2015**, *106*, 203301.
- [25] G. Lu, J. Blakesley, S. Himmelberger, P. Pingel, J. Frisch, I. Lieberwirth, I. Salzmann, M. Oehzelt, R. Di Pietro, A. Salleo, N. Koch, D. Neher, *Nat. Commun.* **2013**, *4*, 1588.
- [26] A. M. Glaudell, J. E. Cochran, S. N. Patel, M. L. Chabiny, *Adv. Energy Mater.* **2015**, *5*, 1401072.
- [27] S. N. Patel, A. M. Glaudell, D. Kiefer, M. L. Chabiny, *ACS Macro Lett.* **2016**, *5*, 268.
- [28] C. Yoon, M. Reghu, D. Moses, A. Heeger, Y. Cao, T.-A. Chen, X. Wu, R. Rieke, *Synth. Met.* **1995**, *75*, 229.
- [29] S. Ukai, H. Ito, K. Marumoto, S.-i. Kuroda, *J. Phys. Soc. Jpn.* **2005**, *74*, 3314.
- [30] H. Koizumi, H. Dougauchi, T. Ichikawa, *J. Phys. Chem. B* **2005**, *109*, 15288.
- [31] Y. Wang, M. Rubner, *Synth. Met.* **1990**, *39*, 153.
- [32] M. R. Bryce, L. C. Murphy, *Nature* **1984**, *309*, 119.
- [33] I. Salzmann, G. Heimel, *J. Electron Spectrosc. Relat. Phenom.* **2015**, *204*, 208.
- [34] R. Lazzaroni, M. Lögdlund, S. Stafström, W. R. Salaneck, J. L. Brédas, *J. Chem. Phys.* **1990**, *93*, 4433.
- [35] V. I. Arkhipov, E. V. Emelianova, P. Heremans, H. Bässler, *Phys. Rev. B* **2005**, *72*, 235202.
- [36] O. Khatib, B. Lee, J. Yuen, Z. Q. Li, M. Di Ventra, A. J. Heeger, V. Podzorov, D. N. Basov, *J. Appl. Phys.* **2010**, *107*, 123702.
- [37] P. Pingel, D. Neher, *Phys. Rev. B* **2013**, *87*, 115209.
- [38] D. T. Duong, C. Wang, E. Antono, M. F. Toney, A. Salleo, *Org. Electron.* **2013**, *14*, 1330.
- [39] J. E. Cochran, M. J. N. Junk, A. M. Glaudell, P. L. Miller, J. S. Cowart, M. F. Toney, C. J. Hawker, B. F. Chmelka, M. L. Chabiny, *Macromolecules* **2014**, *47*, 6836.
- [40] D. T. Duong, H. Phan, D. Hanifi, P. S. Jo, T.-Q. Nguyen, A. Salleo, *Adv. Mater.* **2014**, *26*, 6069.
- [41] D. Di Nuzzo, C. Fontanesi, R. Jones, S. Allard, I. Dumsch, U. Scherf, E. von Hauff, S. Schumacher, E. Da Como, *Nat. Commun.* **2015**, *6*, 6460.
- [42] C. Wang, D. T. Duong, K. Vandewal, J. Rivnay, A. Salleo, *Phys. Rev. B* **2015**, *91*, 085205.
- [43] F. Deschler, D. Riedel, A. Deák, B. Ecker, E. von Hauff, E. Da Como, *Synth. Met.* **2015**, *199*, 381.
- [44] I. Salzmann, G. Heimel, M. Oehzelt, S. Winkler, N. Koch, *Acc. Chem. Res.* **2016**, *49*, 370.
- [45] J. Gao, B. W. Stein, A. K. Thomas, J. A. Garcia, J. Yang, M. L. Kirk, J. K. Grey, *J. Phys. Chem. C* **2015**, *119*, 16396.
- [46] L. Müller, D. Nanova, T. Glaser, S. Beck, A. Pucci, A. K. Kast, R. R. Schröder, E. Mankel, P. Pingel, D. Neher, W. Kowalsky, R. Lovrincic, *Chem. Mater.* **2016**, *28*, 4432.
- [47] D. T. Scholes, S. A. Hawks, P. Y. Yee, H. Wu, J. R. Lindemuth, S. H. Tolbert, B. J. Schwartz, *J. Phys. Chem. Lett.* **2015**, *6*, 4786.
- [48] A. Hamidi-Sakr, L. Biniek, J.-L. Bantignies, D. Maurin, L. Herrmann, N. Leclerc, P. Lévêque, V. Vijayakumar, N. Zimmermann, M. Brinkmann, *Adv. Funct. Mater.* **2017**, *27*, 1700173.
- [49] J. Gao, E. T. Niles, J. K. Grey, *J. Phys. Chem. Lett.* **2013**, *4*, 2953.
- [50] J. Gao, J. D. Roehling, Y. Li, H. Guo, A. J. Moulé, J. K. Grey, *J. Mater. Chem. C* **2013**, *1*, 5638.
- [51] I. E. Jacobs, E. W. Aasen, J. L. Oliveira, T. N. Fonseca, J. D. Roehling, J. Li, G. Zhang, M. P. Augustine, M. Mascal, A. J. Moulé, *J. Mater. Chem. C* **2016**, *4*, 3454.
- [52] J. Li, C. W. Rochester, I. E. Jacobs, E. W. Aasen, S. Friedrich, P. Stroeve, A. J. Moulé, *Org. Electron.* **2016**, *33*, 23.
- [53] J. Li, C. W. Rochester, I. E. Jacobs, S. Friedrich, P. Stroeve, M. Riede, A. J. Moulé, *ACS Appl. Mater. Interfaces* **2015**, *7*, 28420.
- [54] K. Kang, S. Watanabe, K. Broch, A. Sepe, A. Brown, I. Nasrallah, M. Nikolka, Z. Fei, M. Heeney, D. Matsumoto, K. Marumoto, H. Tanaka, S.-i. Kuroda, H. Sirringhaus, *Nat. Mater.* **2016**, *15*, 896.
- [55] Y. Xuan, X. Liu, S. Desbief, P. Leclère, M. Fahlman, R. Lazzaroni, M. Berggren, J. Cornil, D. Emin, X. Crispin, *Phys. Rev. B* **2010**, *82*, 115454.
- [56] A. L. Ayzner, C. J. Tassone, S. H. Tolbert, B. J. Schwartz, *J. Phys. Chem. C* **2009**, *113*, 20050.
- [57] J. C. Aguirre, S. A. Hawks, A. S. Ferreira, P. Yee, S. Subramanian, S. A. Jenekhe, S. H. Tolbert, B. J. Schwartz, *Adv. Energy Mater.* **2015**, *5*, 1402020.
- [58] G. Zhang, R. C. Huber, A. S. Ferreira, S. D. Boyd, C. K. Luscombe, S. H. Tolbert, B. J. Schwartz, *J. Phys. Chem. C* **2014**, *118*, 18424.
- [59] S. A. Hawks, J. C. Aguirre, L. T. Schelhas, R. J. Thompson, R. C. Huber, A. S. Ferreira, G. Zhang, A. A. Herzing, S. H. Tolbert, B. J. Schwartz, *J. Phys. Chem. C* **2014**, *118*, 17413.
- [60] A. S. Ferreira, J. C. Aguirre, S. Subramanian, S. A. Jenekhe, S. H. Tolbert, B. J. Schwartz, *J. Phys. Chem. C* **2016**, *120*, 22115.
- [61] J. J. van Franeker, S. Kouijzer, X. Lou, M. Turbiez, M. M. Wienk, R. A. J. Janssen, *Adv. Energy Mater.* **2015**, *5*, 1500464.
- [62] V. V. Kislyuk, O. P. Dimitriev, A. A. Pud, J. Lautru, I. Ledoux-Rak, *J. Phys.: Conf. Ser.* **2011**, *286*, 012009.
- [63] L. Zhu, E.-G. Kim, Y. Yi, J.-L. Brédas, *Chem. Mater.* **2011**, *23*, 5149.
- [64] J.-F. Chang, B. Sun, D. W. Breiby, M. M. Nielsen, T. I. Sølling, M. Miles, I. McCulloch, H. Sirringhaus, *Chem. Mater.* **2004**, *16*, 4772.
- [65] H. A. Bronstein, C. K. Luscombe, *J. Am. Chem. Soc.* **2009**, *131*, 12894.
- [66] K. A. Mazzio, A. H. Rice, M. M. Durban, C. K. Luscombe, *J. Phys. Chem. C* **2015**, *119*, 14911.
- [67] H. Yang, T. J. Shin, L. Yang, K. Cho, C. Y. Ryu, Z. Bao, *Adv. Funct. Mater.* **2005**, *15*, 671.
- [68] G. Li, V. Shrotriya, J. Huang, Y. Yao, T. Moriarty, K. Emery, Y. Yang, *Nat. Mater.* **2005**, *4*, 864.
- [69] E. Verploegen, R. Mondal, C. J. Bettinger, S. Sok, M. F. Toney, Z. Bao, *Adv. Funct. Mater.* **2010**, *20*, 3519.
- [70] M. Brinkmann, J.-C. Wittmann, *Adv. Mater.* **2006**, *18*, 860.
- [71] H. Méndez, G. Heimel, S. Winkler, J. Frisch, A. Opitz, K. Sauer, B. Wegner, M. Oehzelt, C. Röthel, S. Duhm, D. Többsens, N. Koch, I. Salzmann, *Nat. Commun.* **2015**, *6*, 8560.
- [72] T. F. Harrelson, Y. Q. Cheng, J. Li, I. E. Jacobs, A. J. Ramirez-Cuesta, R. Faller, A. J. Moulé, *Macromolecules* **2017**, *50*, 2424.
- [73] J. Gao, E. T. Niles, J. K. Grey, *J. Phys. Chem. Lett.* **2013**, *4*, 2953.
- [74] F. C. Spano, *J. Chem. Phys.* **2005**, *122*, 234701.
- [75] J. Clark, J.-F. Chang, F. C. Spano, R. H. Friend, C. Silva, *Appl. Phys. Lett.* **2009**, *94*, 163306.
- [76] M. Wohlgenannt, X. M. Jiang, Z. V. Vardeny, *Phys. Rev. B* **2004**, *69*, 241204.
- [77] P. J. Brown, H. Sirringhaus, M. Harrison, M. Shkunov, R. H. Friend, *Phys. Rev. B* **2001**, *63*, 125204.
- [78] T. H. Le, A. Nafady, X. Qu, L. L. Martin, A. M. Bond, *Anal. Chem.* **2011**, *83*, 6731.
- [79] R. Ghosh, C. M. Pochas, F. C. Spano, *J. Phys. Chem. C* **2016**, *120*, 11394.
- [80] C. M. Pochas, F. C. Spano, *J. Chem. Phys.* **2014**, *140*, 244902.
- [81] Y. Nagata, C. Lennartz, *J. Chem. Phys.* **2008**, *129*, 034709.
- [82] H. Sirringhaus, P. J. Brown, R. H. Friend, M. M. Nielsen, K. Bechgaard, B. M. W. Langeveld-Voss, A. J. H. Spiering, R. A. J. Janssen, E. W. Meijer, P. Herwig, D. M. de Leeuw, *Nature* **1999**, *401*, 685.

- [83] H. Sirringhaus, *Adv. Mater.* **2005**, *17*, 2411.
- [84] V. Coropceanu, J. Cornil, D. A. da Silva Filho, Y. Olivier, R. Silbey, J.-L. Brédas, *Chem. Rev.* **2007**, *107*, 926.
- [85] A. Salleo, R. J. Kline, D. M. DeLongchamp, M. L. Chabinyc, *Adv. Mater.* **2010**, *22*, 3812.
- [86] R. Noriega, J. Rivnay, K. Vandewal, F. P. V. Koch, N. Stingelin, P. Smith, M. F. Toney, A. Salleo, *Nat. Mater.* **2013**, *12*, 1038.
- [87] H. Sirringhaus, *Adv. Mater.* **2014**, *26*, 1319.
- [88] L. J. van der Pauw, *Philips Res. Rep.* **1958**, *13*, 1.
- [89] J. Lindemuth, S.-I. Mizuta, *Proc. SPIE* **2011**, *8110*, 81100I.
- [90] J. Lindemuth, *Proc. SPIE* **2012**, *8470*, 84700G.
- [91] Y. Chen, H. T. Yi, V. Podzorov, *Phys. Rev. Appl.* **2016**, *5*, 034008.
- [92] H. T. Yi, Y. N. Gartstein, V. Podzorov, *Sci. Rep.* **2016**, *6*, 23650.
- [93] S. Wang, M. Ha, M. Manno, C. Daniel Frisbie, C. Leighton, *Nat. Commun.* **2012**, *3*, 1210.
- [94] Z. Bao, A. Dodabalapur, A. J. Lovinger, *Appl. Phys. Lett.* **1996**, *69*, 4108.
- [95] M. Brinkmann, P. Rannou, *Adv. Funct. Mater.* **2007**, *17*, 101.
- [96] R. K. Singh, J. Kumar, R. Singh, R. Kant, S. Chand, V. Kumar, *Mater. Chem. Phys.* **2007**, *104*, 390.
- [97] A. L. Efros, B. I. Shklovskii, *J. Phys. C: Solid State Phys.* **1975**, *8*, L49.
- [98] N. Mott, *J. Non. Cryst. Solids* **1968**, *1*, 1.